Tolerant Sequential Model Predictive Control Based on Lexicographic Optimization Method for T-Type Three-Phase Three-Level Inverters

Shengwei Chen, Yong Yang, *Senior Member, IEEE*, Rong Chen, Jiefeng Hu, *Senior Member, IEEE*, Huiqing Wen, *Senior Member, IEEE*, Yiwang Wang, *Member, IEEE*, Weimin Wu, *Member, IEEE*, Gang Fang, *Member, IEEE*, and Jose Rodriguez, *Life Fellow, IEEE*

***Abstract*—Due to the existence of the neutral point (NP) voltage, controlling the three-level inverters has essentially become a multiobjective optimization problem (MOOP) that needs to provide stable output voltages for the load and maintain the NP voltage simultaneously. Traditionally, this MOOP is converted into a single-objective optimization problem by weighting factors. However, since the physical dimensions of the two control objectives are usually different, it is challenging to choose proper weighting factors to obtain a satisfactory performance according to a specific theory. To address this issue, a tolerant sequential model predictive control (TSMPC) utilizing a lexicographic optimization method is proposed in this article. This method establishes two distinct layers for the output voltage and NP voltage, arranging them in sequence according to the importance of control objectives to evaluate all voltage vectors. By using an explainable tolerance value rather than conventional weighting factors, the proposed TSMPC algorithm presents superior performance over traditional MPC approaches. Finally, the feasibility and effectiveness of the proposed TSMPC algorithm have been verified through relevant experiments and the stability of this algorithm has also been analyzed.**

***Index Terms*—Lexicographic optimization method, model predictive control (MPC), multiobjective optimization problem (MOOP), weighting factors.**

Received 6 September 2024; accepted 26 October 2024. Date of publication 4 November 2024; date of current version 18 December 2024. This work was supported in part by the National Natural Science Foundation of China under Grant 52377195, in part by the Transformation of Scientific and Technological Achievements in Suzhou (Carbon Peak Carbon Neutral Project) under Grant ST202303, in part by CONICYT Projects FB0008, ACT192013 and 1170167, in part by the Suzhou Key Laboratory of Smart Energy Technology, in part by the Science and Technology Planning Project of Suzhou City under Grant SZS2022015 and Grant 2022SS39, and in part by the Project for constructing an excellent teaching team by "Qing Lan Project" of the Education Department of Jiangsu Province:2023. Recommended for publication by Associate Editor M. Hagiwara. *(Corresponding authors: Yong Yang; Rong Chen.)*

Shengwei Chen is with the School of Rail Transportation, Soochow University, Suzhou 215131, China, and also with the College of Electrical Engineering, Zhejiang University, Hangzhou 310027, China (e-mail: chenshengwei@zju.edu.cn).

Yong Yang and Rong Chen are with the School of Rail Transportation, Soochow University, Suzhou 215131, China, and also with the Intelligent Urban Rail Engineering Research Center of Jiangsu Province, Suzhou 215131, China (e-mail: yangy1981@suda.edu.cn; chrong@suda.edu.cn).

Jiefeng Hu is with the Centre for New Energy Transition Research, Federation University Australia, Mount Helen, VIC 3353, Australia, and also with the Institute of Innovation, Science and Sustainability, Federation University Australia, Mount Helen, VIC 3353, Australia (e-mail: j.hu@federation.edu.au).

Huiqing Wen is with the Department of Electrical and Electronic Engineering, Xi'an Jiaotong-Liverpool University, Suzhou 215123, China (e-mail: huiqing.wen@xjtlu.edu.cn).

Yiwang Wang is with the Collaborative Innovation Center of Smart Energy Equipment and Power Conversion, Suzhou Vocational University, Suzhou 215104, China (e-mail: wyiwang@163.com).

Weimin Wu is with the Department of Electrical Engineering, Shanghai Maritime University, Shanghai 201306, China (e-mail: wmwu@shmtu.edu.cn).

Gang Fang is with the GOODWE Technology Company, Ltd., Suzhou 215100, China (e-mail: kevin.fang@goodwe.com).

Jose Rodriguez is with the Faculty of Engineering, Universidad San Sebastian Santiago, Santiago 8370146, Chile (e-mail: jose.rodriguezp@uss.cl).

Color versions of one or more figures in this article are available at https://doi.org/10.1109/TPEL.2024.3490654.

Digital Object Identifier 10.1109/TPEL.2024.3490654

I. Introduction

AMIDST the global shift towards low-carbon energy and the pursuit of carbon neutrality, transitioning the energy landscape of the transportation and power generation sectors is extremely crucial. Because these two sectors are significant consumers of conventional fossil fuels, research into transportation electrification and renewable energy generation technologies has become very popular [1], [2], [3], [4]. Inverters, as the critical link between dc and ac systems, have emerged as vital components in renewable energy generation systems and electric vehicles [5], [6]. Meanwhile, strategies for controlling inverters have been explored continuously. Proportional-integral control, a linear control algorithm, is widely used in industry due to its relatively simple control principles and low computational requirements [7], [8], [9], [10]. However, there exists a trade-off between the steady-state and dynamic performances of this algorithm. In addition, the inadequate performance of systems with strong nonlinearity, which proves challenging to approximate linearly, is also a significant issue that cannot be overlooked [11], [12]. As the pursuit of better performance on nonlinear systems intensifies, and thanks to the enhancement of the computing power of microprocessor chips, model predictive control (MPC) is beginning to be widely used in power electronics because of its good performance on multivariable and nonlinear systems [13], [14], [15].

Compared with conventional two-level inverters, three-level inverters have the advantages of higher efficiency and lower ripple, but they also introduce a new control objective—the neutral point (NP) voltage [16], [17]. Consequently, the control problem becomes a multiobjective optimization problem (MOOP), requiring simultaneous reference voltage tracking and

NP voltage balance maintenance. Generally, MOOPs cannot find an absolute optimal solution in practical applications. The solution to MOOPs is an acceptable relative optimum, which is called a Pareto optimal solution [18]. MPC uses weighting factors to combine two control objectives into a single cost function to solve MOOPs. By modifying the specific values of weighting factors, the performance of the two control objectives can be adjusted [19]. However, since the physical dimensions or magnitudes of the control objectives may be inconsistent, suitable values for the weighting factors can only be determined by extensive experimentation rather than by specific theory, leading to a tedious tuning process [20]. Moreover, the interpretability of conventional MPC is deficient.

In response to the above-mentioned problems caused by the weighting factors, several innovative algorithms have been proposed for the automatic determination of the weighting factors [21], [22]. In [21], a fuzzy optimization approach is combined with MPC to achieve online dynamic adjustment of weighting factors. However, the fuzzy inference rules require a significant amount of prior knowledge acquired through extensive experiments. By combining the sliding mode control with MPC, Oshnoei and Blaabjerg [22] propose a method that can update the weight coefficients online in real time. While this method enhances system robustness, there remains a time-consuming process of tuning multiple parameters involved in the construction of the sliding mode. With the popularity of artificial intelligence research, some intelligent control algorithms, such as particle swarm optimization (PSO), genetic algorithm (GA), and deep learning using an artificial neural network (ANN), have been employed to optimize the selection process of weighting factors [23], [24], [25]. For example, in [23], a PSO is integrated into MPC to realize online automatic updates and adjustments of weighting factors. In [24], a GA is employed to optimize the weighting factors selection process. In [25], an offline method for determining weighting factors with the aid of ANN is proposed by integrating deep learning with MPC. However, the significant drawback of these methods is the excessive computational burden. Besides, since the weighting factors remain and there is no clear explanation of the correlation between the two control objectives, the interpretability of these algorithms has not significantly improved.

Therefore, removing weighting factors in MPC for MOOPs has become an interesting research direction. For the control of the NP voltage, which is a specific control objective in three-level inverters, the commonly used approach for eliminating weighting factors is the application of redundant small voltage vectors (VVs) to dynamically balance the NP voltage. Nevertheless, this method is not intuitive enough and frequently neglects the impact of the medium VV on the NP voltage [26], [27]. An MPC based on the ranking method has been proposed in [28], which excludes weighting factors. The cost functions of each control objective are ranked from smallest to largest, and the VV with the smallest average ranking value of all control objectives is selected as the optimal one. Since the ranking values can only reflect the relative position of deviations under different VVs, there may be situations where the specific error value is small, but the ranking gap is significant. Consequently, the fairness of this evaluation system could be problematic.

On this basis, sequential MPC based on lexicographic optimization has been proposed to eliminate weighting factors [29], [30]. A multilayer serial screening structure is applied to find the optimal VV from the candidates. Each layer of this structure represents a control objective, prioritized according to its importance. And the optimal solution set of each layer serves as the candidate for the next layer. Nevertheless, within this optimization framework, if there exists only one viable solution in the preceding layer, it is deemed the optimal solution for the entire problem, regardless of its effectiveness in addressing subsequent control objectives. This results in an incapacity to effectively fulfill subsequent control objectives. To address this issue, it is necessary to relax the constraint of the nonlast layer to expand the size of the solution set [31], [32]. However, neither of these methods provides a satisfactory explanation of the basis for selecting the number of candidates, which is two in [29] and three in [30]. A new idea of constraint relaxation has been proposed in [33]. Instead of limiting the number of candidates, a tolerance value is introduced to ensure that the solution of the nonlast layers is not unique. However, this method is applied to a two-level permanent magnet synchronous motor platform rather than a three-level inverter. The computational burden will become a significant challenge in three-level inverters due to the exponential increase in the number of candidates resulting from the increase in output level. In addition, the lack of a reasonable explanation of the specific meaning of the tolerance value is also another problem.

Inspired by the above-mentioned methods, this article proposes a tolerant sequential MPC (TSMPC) based on lexicographic optimization to eliminate weighting factors. A two-layer serial screening structure is constructed based on the priority of the control objectives. Specifically, the first layer focuses on the cost function of the output voltage, while the second layer includes a cost function to deal with the NP voltage. During the optimization process of the first layer, the minimum output voltage cost function value is augmented by the tolerance value to create a new constraint. The main contributions of this work are summarized as follows.

1) Compared to the weighting factors in conventional MPC, the tolerance value in the proposed TSMPC has a more intuitive physical meaning, which can be illustrated both graphically and textually. The tolerance value represents the maximum acceptable deviation based on the known minimum deviation, which is related to the performance.
2) The multiple comparison loops in TSMPC are quite time-consuming and can significantly deplete CPU resources. The proposed TSMPC mitigates this by reducing the number of VVs entering multilayer serial structures through sector identification, thereby effectively controlling the increase in computational burden.
3) Compared to the sequential MPC methods presented in [29] and [30] that limit the number of candidate VVs, the proposed TSMPC relaxes the cost function range by a tolerance value, making the number of candidate VVs

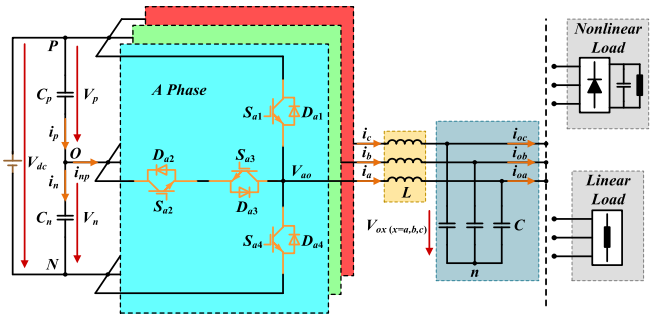

Fig. 1. Topology of the T-type 3P-3L inverter with *LC* filter.

variable. In inverters, especially three-level ones, there may be multiple VVs available for the same voltage. Restricting the number of candidates may result in an overly strict constraint, potentially preventing the identification of the optimal solution. However, the proposed TSMPC can mitigate such issues by constraining the value of the cost function.

4) Because each layer in the proposed TSMPC operates independently and corresponds to a specific control objective, the comparisons within each layer are made between variables with a similar magnitude. Thus, regardless of which control objective undergoes a sudden change, the comparison process in the corresponding layer quickly constrains the error to achieve rapid tracking. As a result, the proposed TSMPC exhibits a superior ability to respond quickly to dynamic changes across all control objectives. This is a significant advantage over conventional MPC with weighting factors and MPC using redundant small VVs.

The rest of this article is organized as follows. Section II describes the mathematical model of the T-type three-phase three-level (3P-3L) inverter. Section III provides a detailed introduction to the basic principle of the lexicographic optimization method. In Section IV, the principles of the conventional FCS-MPC and the proposed TSMPC are given. Specific comparative experimental results are given in Section V, and Section VI concludes this article.

II. Mathematical Model

The topology applied in this article is specifically shown in Fig. 1. On the input side, V_{dc} represents dc-link voltage; C_p and C_n are the upper and lower dc-link capacitors, respectively; V_p, V_n, i_p, and i_n represent their voltages and currents respectively; and i_{np} represents the current flowing out of the NP. On the output side, L is the filter inductance and C is the filter capacitance; $i_{x(x=\,a,b,c)}$ and $V_{xo\,(x=\,a,b,c)}$ respectively represent the inverter output current and voltage; $i_{ox(x=\,a,b,c)}$ and $V_{ox(x=\,a,b,c)}$ respectively represent the current and the voltage of the load. Each phase of the inverter circuit is composed of four power switching devices. For ease of expression, the power switching device can be denoted by S_{xi} where $i \in \{1, \ldots, 4\}$ and $x \in \{a, b, c\}$, and the states "ON" and "OFF" are represented by "1" and "0" respectively. Assuming that the NP voltage can be well balanced, all possible switching states and their corresponding inverter output voltages for each phase under consideration of avoiding direct conduction are shown in Table I. The output state of each phase $S_{x(x=\,a,b,c)}$ can be defined as follows:

TABLE I
Switching States and Inverter Output Voltages

Output state	Switching state				Output voltage
S_x	S_{x1}	S_{x2}	S_{x3}	S_{x4}	V_{xo}
1	1	1	0	0	$V_{dc}/2$
0	0	1	1	0	0
−1	0	0	1	1	$-V_{dc}/2$

$$S_{x(x=a,b,c)} = \begin{cases} 1, & V_{xo} = V_{dc}/2 \\ 0, & V_{xo} = 0 \\ -1, & V_{xo} = -V_{dc}/2 \end{cases}. \tag{1}$$

The relationship between the load voltage, also known as the output phase voltage, and the inverter output voltage can be expressed as follows:

$$\begin{cases} V_{an} = V_{ao} - V_{no} \\ V_{bn} = V_{bo} - V_{no} \\ V_{cn} = V_{co} - V_{no} \end{cases}, \quad V_{no} = \frac{V_{ao} + V_{bo} + V_{co}}{3}. \tag{2}$$

By (1) and (2), the relationship between the inverter output voltage and the phase output state can be established as

$$\begin{bmatrix} V_{an} \\ V_{bn} \\ V_{cn} \end{bmatrix} = \frac{V_{dc}}{6} \begin{bmatrix} 2 & -1 & -1 \\ -1 & 2 & -1 \\ -1 & -1 & 2 \end{bmatrix} \begin{bmatrix} S_a \\ S_b \\ S_c \end{bmatrix}. \tag{3}$$

To facilitate analysis and study, the abc frame is transformed to the $\alpha\beta$ frame using the amplitude-invariant Clarke transformation. Then, in the $\alpha\beta$ frame, the inverter output current i and voltage V, as well as the load current i_o and voltage V_o, can be represented as

$$\begin{cases} i = i_\alpha + j i_\beta = K \begin{bmatrix} i_a & i_b & i_c \end{bmatrix}^T \\ V = V_\alpha + j V_\beta = K \begin{bmatrix} V_{an} & V_{bn} & V_{cn} \end{bmatrix}^T \\ i_o = i_{o\alpha} + j i_{o\beta} = K \begin{bmatrix} i_{oa} & i_{ob} & i_{oc} \end{bmatrix}^T \\ V_o = V_{o\alpha} + j V_{o\beta} = K \begin{bmatrix} V_{oa} & V_{ob} & V_{oc} \end{bmatrix}^T \end{cases},$$

$$K = \frac{2}{3} \begin{bmatrix} 1 & -1/2 & -1/2 \\ 0 & \sqrt{3}/2 & -\sqrt{3}/2 \end{bmatrix}. \tag{4}$$

By combining the three-phase output state ($S_a\, S_b\, S_c$), 27 (3^3) VVs can be obtained in a T-type 3P-3L inverter. The space VVs diagram of the 27 VVs is shown in Fig. 2. The amplitude and positional information can be intuitively reflected in Fig. 2. Thus, based on this information, 27 VVs can be simply classified and categorized. Based on the magnitude, they can be divided into large VV, medium VV, small VV, and zero VV. In addition, based on the position, they can also be divided into six sectors.

By analyzing the filter capacitor and inductor, which are considered dynamic components, the differential equations for

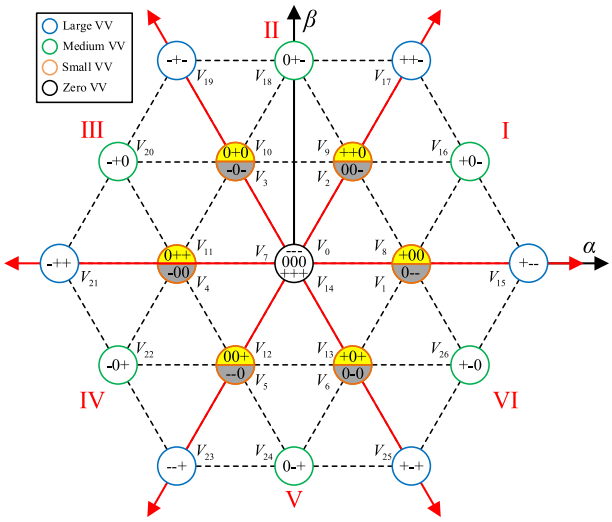

Fig. 2. Space VVs diagram of 27 VVs.

the load voltage and the inverter output current are derived

$$\frac{dV_o}{dt} = \frac{1}{C_f}(i - i_o) \tag{5}$$

$$\frac{di}{dt} = \frac{1}{L}(V - V_o). \tag{6}$$

Based on (5) and (6), the state-space equations of the system can be expressed as

$$\begin{aligned} \dot{x} &= \boldsymbol{A}x + \boldsymbol{B}u + \boldsymbol{C}n \\ y &= \boldsymbol{D}x \end{aligned} \tag{7}$$

where state vector $x = [V_o \quad i]^T$, input vector $u = [V \quad 0]^T$, vector $n = [i_o \quad 0]^T$, output $y = V_o$ and

$$\boldsymbol{A} = \begin{bmatrix} 0 & 1/C \\ -1/L & 0 \end{bmatrix}, \quad \boldsymbol{B} = \begin{bmatrix} 0 & 0 \\ 1/L & 0 \end{bmatrix},$$
$$\boldsymbol{C} = \begin{bmatrix} -1/C & 0 \\ 0 & 0 \end{bmatrix}, \quad \boldsymbol{D} = \begin{bmatrix} 1 \\ 0 \end{bmatrix}. \tag{8}$$

If the sampling time of the system is denoted by T_s, then (5) can be discretized using the Euler method as

$$\begin{aligned} x(k+1) &= (\boldsymbol{I}_{2\times 2} + T_s\boldsymbol{A})x(k) + T_s\boldsymbol{B}u(k) + T_s\boldsymbol{C}n(k) \\ y(k) &= \boldsymbol{D}x(k). \end{aligned} \tag{9}$$

However, it is important to note that (9) can only be used to predict the inverter current i based on the switching state, rather than the load voltage V_o. Therefore, further revision is necessary. Electricity is essentially the movement of electrons. It is evident that the inverter current changes first, followed by the load voltage. Therefore, $i(k+1)$ can be considered the instantaneous inverter output current at instant k. The prediction formula can be modified as

$$x(k+1) = \boldsymbol{A}'x(k) + \boldsymbol{B}'u(k) + \boldsymbol{C}'n(k) \tag{10}$$

where

$$\boldsymbol{A}' = \begin{bmatrix} 1 - \frac{T_s^2}{LC} & \frac{T_s}{C} \\ -\frac{T_s}{L} & 1 \end{bmatrix}, \boldsymbol{B}' = \begin{bmatrix} \frac{T_s^2}{LC} & 0 \\ \frac{T_s}{L} & 0 \end{bmatrix}, \boldsymbol{C}' = \begin{bmatrix} -\frac{T_s}{C} & 0 \\ 0 & 0 \end{bmatrix}. \tag{11}$$

III. Principle of Lexicographic Optimization Method

A. Definitions and Preliminaries

The control of a t-type 3P-3L inverter, which needs to track the reference voltage and maintain the NP voltage is essentially a MOOP. A general expression of (10) can be modified as

$$x(k+1) = f(x(k), u(k)), k = 0, 1, 2, \ldots \tag{12}$$

$$x(k) \in X, u(k) \in U \forall k = 0, 1, 2, \ldots \tag{13}$$

where $x(k) \in R^n$ is the state variable at instant k, $u(k) \in R^n$ is the control variable at instant k, and $f(\cdot,\cdot)$ is a locally Lipschitz function of $x(k)$ and $u(k)$ with $f(0,0) = 0$. The model (12) is constrained by state and control variable constraints (13). $X \subset R^n$ is a closed set and $U \subset R^n$ is a compact set, both of which consist of the origin.

For convenience, $x(k)$ and $u(k)$ can be abbreviated as x_k, u_k. Furthermore, the selection of u_k is limited to the 27 VVs in the 3P-3L inverter. The sequences of future control variables and state variables at instant k can be expanded as

$$u_{N,k} = \{u_{k|k}, u_{k+1|k}, \ldots, u_{k+N-1|k}\} \tag{14}$$

$$x_{N,k} = \{x_{k|k}, x_{k+1|k}, \ldots, x_{k+N-1|k}, x_{k+N|k}\} \tag{15}$$

where$N \geq 1$ represents the prediction horizon, $u_{k+i|k}$ represents the control voltage at instant $k + i$, $i = 0, \ldots, N-1$. $x_{k+j|k}$ represents the predicted state at instant $k+j$, $j = 0, \ldots, N-1$ with the state $x_k = x_{k|k}$ and input $u_{N,k}$ applied in the predicted model (12) at instant k. Considering the number of the system control objectives $m \geq 2$, the cost functions can be expressed as

$$J_i(u_{N,k}, x_k) = E_i(x_{k+N|k}) + \sum_{j=0}^{N-1} L_i(u_{k+j|k}, x_{k+j|k})$$
$$i = 1, 2, \ldots, m \tag{16}$$

where $L_i : U \times X \to \mathrm{R}$ and $E_i : X \to \mathrm{R}$are the stage costs and terminal costs of the control objective i respectively. The MOOP can be expressed as

$$\min_{u_{N,k}} J(u_{N,k}, x_k) = [J_1(u_{N,k}, x_k), \ldots, J_m(u_{N,k}, x_k)] \tag{17}$$

$$\text{s.t. } x_{k+j|k} = f(x_{k+j-1|k}, u_{k+j-1|k}), x_{k|k} = x_k$$
$$x_{k+j|k} \in X, u_{k+j-1|k} \in U, j = 1, \ldots, N. \tag{18}$$

To solve MOOPs, it is necessary to simultaneously minimize m different cost functions, which has been very challenging in practice.

B. Lexicographic Optimal Solution for MOOPs

The most common method for solving MOOPs is to transform them into single-objective optimization problems by introducing weighting factors. However, the weighting factors of this method can be cumbersome to adjust and difficult to interpret. Another option for MOOPs is lexicographic optimization [31], [32]. This method constructs a multilayer serial screening structure to find the optimal solution. Each layer has its own constraints to find its solution set. The optimal solution set for each layer is used as the candidate for the next layer. In addition, the layers are sequenced based on the priority of the control objectives: the layer with the highest priority is placed first and the layer with the lowest priority is positioned at the end. For simplicity, $J_i(u_{N,k}, x_k)$ is denoted as J_i, $i = 1, 2, \ldots, m$. Assuming the cost functions have been sequenced by priority, the optimal value of each can be expressed as

$$J_1^* = \min_{u_{N,k}} \{ J_1 | (18) \} \tag{19}$$

$$J_i^* = \min_{u_{N,k}} \left\{ J_2 | \begin{matrix} (18), J_j = J_j^* \\ \forall j = 1, \ldots, i-1 \end{matrix} \right\}, i = 2, \ldots, m-1. \tag{20}$$

Then, the lexicographic optimal solution can be formulated as

$$u_{N,k}^* = \operatorname{argmin} \left\{ J_m | \begin{matrix} (18), J_j = J_j^* \\ \forall j = 1, \ldots, i-1 \end{matrix} \right\}. \tag{21}$$

The basic principle of this method is described as follows. The original constraints are used to minimize the first cost function. Then, the cost function of the subsequent layer is minimized in the previous solution set, effectively treating it as an additional constraint. This sequential process continues until reaching the second-to-last (m-1th) layer. Finally, the lexicographic optimal solution can be found by minimizing the cost function of the last (mth) layer in the solution set of the second-to-last (m-1th) layer.

However, if there is only one feasible solution in the solution set of a layer excluding the last layer, it will render the following optimization process meaningless. To address this issue, it is necessary to introduce a tolerance into the additional constraint $J_j = J_j^*$.

$$J_j \le J_j^* + \varepsilon_j, \forall j = 1, \ldots, k-1 \tag{22}$$

where $\varepsilon_j \ge 0$ denotes the tolerance. The process of the lexicographic method with tolerances is illustrated in Fig. 3.

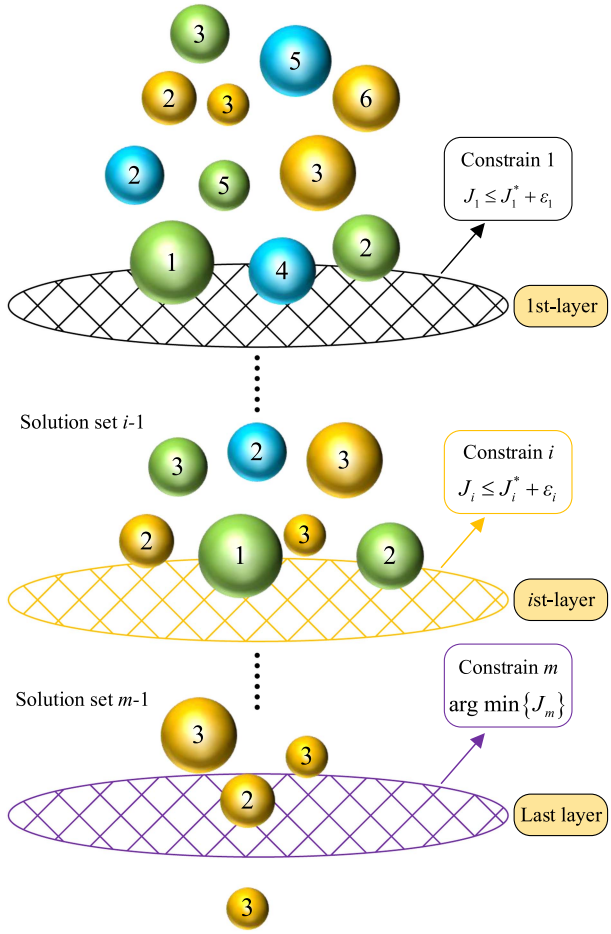

Fig. 3. Schematic diagram of the lexicographic method with tolerances.

IV. Principle of Control Algorithm

This article discusses the control of the 3P-3L inverter to simultaneously track the reference voltage and control the NP voltage, which is a typical MOOP. A TSMPC based on the lexicographic optimization method has been proposed. This method not only eliminates the cumbersome regulation process in the conventional MPC with weighting factors but also makes the NP voltage control more intuitive compared with the MPC using redundant small VVs to dynamically maintain NP balance. Moreover, the proposed method shows superior interpretability of tolerance values, which are difficult to achieve by using conventional MPC algorithms.

A. Conventional MPC With Weighting Factors

Based on (10), the load voltage prediction formula can be expressed as

$$\begin{aligned} V_{o\alpha,k+1} &= \left(1 - \frac{T_s^2}{LC}\right) V_{o\alpha,k} + \frac{T_s}{C} i_{\alpha,k} + \frac{T_s^2}{LC} V_{\alpha,k} - \frac{T_s}{C} i_{o\alpha,k} \\ V_{o\beta,k+1} &= \left(1 - \frac{T_s^2}{LC}\right) V_{o\beta,k} + \frac{T_s}{C} i_{\beta,k} + \frac{T_s^2}{LC} V_{\beta,k} - \frac{T_s}{C} i_{o\beta,k}. \end{aligned} \tag{23}$$

The cost function J_{out} of the load voltage, which is the first control objective is designed as follows:

$$J_{\text{out}} = (V_{o\alpha}^* - V_{o\alpha,k+1})^2 + (V_{o\beta}^* - V_{o\beta,k+1})^2. \tag{24}$$

In 3L inverters, it is necessary to predict and control the NP voltage because of the charging and discharging process of the upper and lower dc-link capacitors during operation. In Fig. 1, the upper and lower dc-link capacitor currents i_p and i_n can be

respectively expressed as

$$i_p = C_p \frac{dV_p}{dt}, \quad i_n = C_n \frac{dV_n}{dt} \tag{25}$$

where $C_p = C_n = C_{np}$. Discretizing (25) using the forward Euler

$$V_{p,k+1} = V_{p,k} + \frac{T_S}{C_{np}} i_{p,k}, V_{n,k+1} = V_{n,k} + \frac{T_S}{C_{np}} i_{n,k}. \tag{26}$$

Analyzing at neutral O, the NP current i_{np} can be expressed in two ways

$$i_{np} = (1 - |S_a|)i_a + (1 - |S_b|)i_b + (1 - |S_c|)i_c \tag{27}$$

$$i_{np} = i_p - i_n. \tag{28}$$

Obviously, the relationship between the NP current i_{np} and the phase output states can be established by (27). Based on (26), the prediction formula for the deviation of the upper and lower dc-link capacitor voltages V_{diff} at instant $k+1$ can be obtained as

$$V_{diff,k+1} = V_{p,k+1} - V_{n,k+1} = V_{p,k} - V_{n,k} + \frac{T_S}{C_{np}} i_{np}. \tag{29}$$

The cost function J_{np} of the NP voltage which is the second control objective is designed as follows:

$$J_{np} = \left(V_{p,k} - V_{n,k} + \frac{T_S}{C_{np}} i_{np} \right)^2. \tag{30}$$

The conventional MPC (C-MPC) uses the weighting factor λ to combine two control objectives into a single cost function to solve the MOOPs. The cost function of C-MPC is designed as

$$J_{\text{C-MPC}} = J_{\text{out}} + \lambda J_{np}. \tag{31}$$

B. MPC Using Redundant Small VVs

The tedious tuning process of weighting factors in C-MPC has been a challenge. An MPC using redundant small VVs (SVV-MPC) has been proposed to eliminate weighting factors [26], [27]. In contrast to C-MPC, SVV-MPC implements the NP voltage control by modifying candidate VVs instead of modifying the cost function. Thus, the cost function of SVV-MPC is designed as

$$J_{\text{SVV-MPC}} = J_{\text{out}}. \tag{32}$$

For all 27 VVs, only small and medium VVs have effects on the NP voltage, while large and zero VVs do not. Redundant small VVs can be classified as positive or negative types based on their impact on the NP voltage. Positive small VVs shown in yellow decrease V_p and increase V_n, while negative small VVs shown in grey increase V_p and decrease V_n. It can be noticed from Fig. 2 that the positive and negative small VVs appear in pairs. Utilizing this characteristic, the NP voltage can be controlled by modifying the candidate VVs. The candidate VVs are constructed as shown in Fig. 4. The negative small VVs are eliminated from all 27 VVs when $V_p > V_n$, while the positive small VVs are eliminated conversely. By this method, dynamic balancing of the NP voltage can be achieved without changing the cost function.

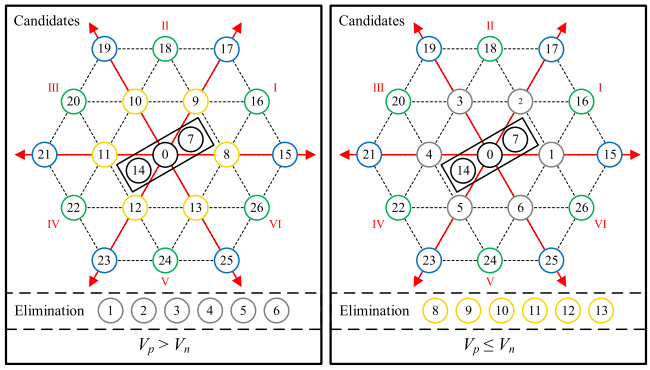

Fig. 4. Composition diagram of candidate VVs.

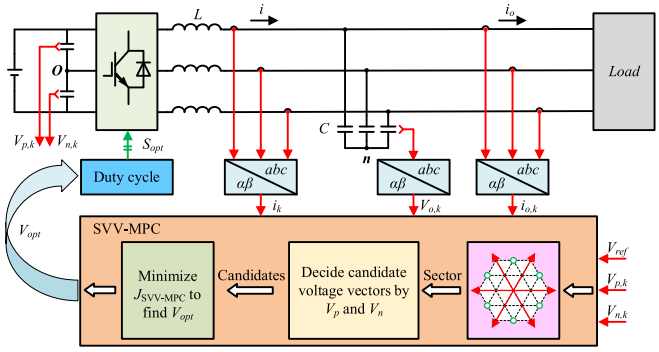

Fig. 5. Block diagram of SVV-MPC.

The specific control block diagram of the SVV-MPC is illustrated in Fig. 5. Initially, the candidate sector is identified by minimizing the $J_{\text{SVV-MPC}}$ of medium VVs. Subsequently, the candidate VVs are decided in accordance with the magnitudes of V_p and V_n. Finally, by minimizing the $J_{\text{SVV-MPC}}$, the optimal VV is selected from the set of candidate VVs and then applied to the inverter.

C. Proposed TSMPC

The SVV-MPC does not consider the effects of the medium VVs on the NP voltage, which restricts its NP voltage balancing capability. Thus, a TSMPC has been proposed. Based on the priority of the control objectives, tracking the reference voltage is placed in the first layer, while maintaining the NP voltage is placed in the second layer. The cost functions of the first and second layers can be respectively expressed as

$$J_1 = J_{\text{out}} \tag{33}$$

$$J_2 = J_{np}. \tag{34}$$

The first layer of TSMPC is dedicated to assessing the deviation in tracking the reference load voltage. In this layer, the minimum cost function J_1^* is identified by evaluating the first cost function J_1 across 27 VVs. Subsequently, based on the principle of the lexicographic optimization method outlined in Section III, a tolerance ε is introduced to relax the constraint of the first layer, thereby ensuring the subsequent optimization

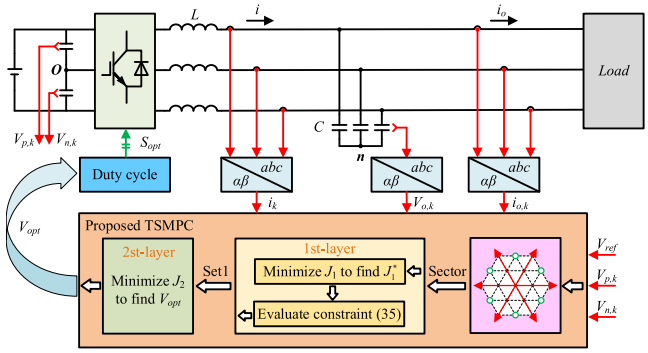

Fig. 6. Block diagram of the proposed TSMPC.

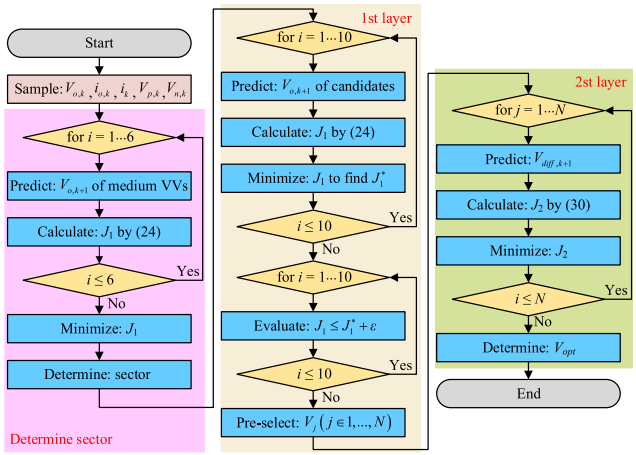

Fig. 7. Flowchart of the proposed TSMPC.

process remains both feasible and meaningful. The modified first-layer constraint can be expressed as follows:

$$J_1 \le J_1^* + \varepsilon. \tag{35}$$

Then, the 27 VVs are re-evaluated in accordance with the modified constraint (35), and those that satisfy this constraint are selected as candidates for the second layer.

The second layer of TSMPC is dedicated to assessing the NP voltage. Based on the NP voltage deviation prediction formula shown in (29), the VV with the minimum J_2 is identified from all candidate VVs and determined as the optimal VV to be applied to the inverter.

It noted that in 3L-3P inverters, the first layer in TSMPC needs to evaluate the 27 VVs twice. The first evaluation is to identify J_1^*, while the second is to find the VVs satisfying (35). This significantly consumes CPU resources, thus limiting the practical application of this algorithm.

1) Determine the Sector: To ensure the successful execution of the experiments, it is essential to reduce CPU resource consumption. This can be accomplished by implementing a sector determination process prior to the first layer, which reduces the number of candidate VVs entering the first layer. This process determines the sector by minimizing the cost function of medium VVs and selects the VVs within that sector as candidates for the first layer.

With the introduction of the sector determination process, the proposed TSMPC algorithm only requires to evaluate six medium VVs once and ten candidate VVs within the sector twice during the first layer. This method can significantly reduce the execution time. Furthermore, sector determination imposes a simple constraint on the range of load voltage variation, ensuring that VVs outside the sector are not selected, even if the tolerance value is excessively large. This effectively prevents the potential abnormal increase in total harmonic distortion (THD) under such conditions.

Fig. 6 depicts the block diagram of the proposed TSMPC, while Fig. 7 depicts the corresponding flowchart. The proposed TSMPC can be divided into three parts: sector determination, first-layer screening, second-layer screening. In Part 1, the sector is determined by minimizing J_1 of the medium VVs. In Part 2, the J_1 of the VVs in the determined sector is minimized to find the smallest cost function J_1^*. $J_1^* + \varepsilon$ is used as the maximum

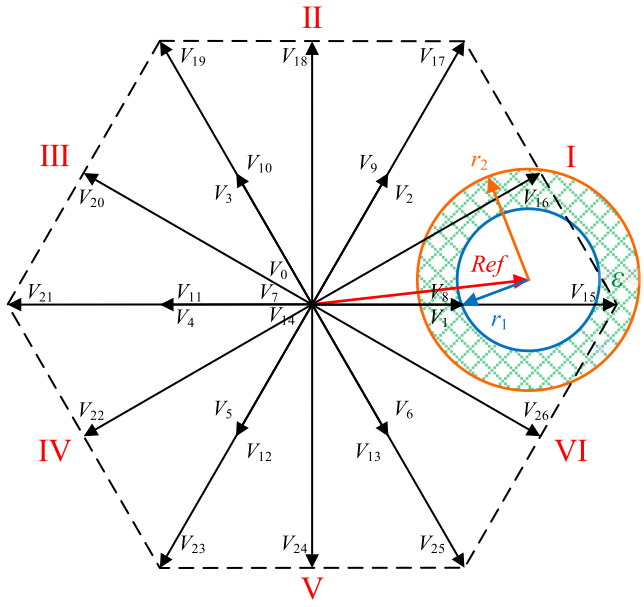

Fig. 8. Schematic diagram explaining the physical meaning of ε.

allowable voltage deviation to evaluate the candidate VVs. The solution set will be candidates for the second layer, where N represents the number of candidates and is a variable. In Part 3, the optimal VV is found by minimizing J_2.

2) Physical Meaning of the Tolerance Value ε: The tolerance value ε is a crucial variable in the proposed TSMPC, which can reflect the range of error tolerance. Fig. 8 is the schematic diagram explaining the physical meaning of the tolerance value ε, where the red arrow represents the load voltage reference. Based on (24), the cost function J_1 is similar to Euclidean distance formula, indicating the voltage deviation between the reference voltage and the candidate VV. This is analogous to drawing a circle $\odot 1$ with r_1 as its radius while the reference voltage pointing to its center, where $r_1^2 = J_1^*$. The relaxed constraint (35) implies that any VV with a voltage deviation less than $J_1^* + \varepsilon$ can satisfy the constraint of the first layer. This means that, in

Fig. 8, all VVs within the circle ⊙2 with r_2 as its radius and the reference voltage as the center can pass the first layer, where $r_2^2 = J_1^* + \varepsilon$.

Introducing the tolerance value ε is analogous to enlarging the radius of circle ⊙1 to obtain circle ⊙2, ensuring that more VVs fall within the circle. The green shaded area between circles ⊙1 and ⊙2 in Fig. 8 is the graphical depiction of ε. By adjusting the value of ε, the radius of circle ⊙2 can be modified, effectively altering the maximum allowable voltage deviation. This adjustment regulates the number of VVs that pass the first layer. The aforementioned explanation provides both a graphical and textual explanation of the physical meaning of the tolerance value ε.

3) Advantages of the Proposed TSMPC: Compared to the weighting factors in C-MPC, the tolerance value in the proposed TSMPC has a more intuitive physical meaning, which is a notable advantage of the proposed method. As shown in (31), the C-MPC integrates the control effects of two control objectives through the weighting factors. However, when the magnitude or order of magnitude of the two control objectives differ, the value of the weighting factors cannot be simply understood as the weighting of the two objectives. In contrast, the tolerance value in the proposed TSMPC has an intuitive physical meaning, as graphically and textually described in the part of "*b) The Physical Meaning of the Tolerance Value* ε" in Section IV.

An additional advantage of TSMPC is its superior control performance in handling dynamic changes across all control objectives, characterized by faster response times. Since the weighting factors merely integrate the numerical errors of two control objectives, C-MPC is a simple numerical compromise between two control objectives. Consequently, when the secondary or smaller order of magnitude control objective has a sudden change, its numerical fluctuation appears minor within the overall cost function, leading to poor dynamic tracking performance for that control objective in C-MPC.

Although SVV-MPC can use redundant small VVs to adjust the NP voltage, it lacks the ability to quantitatively differentiate the impact of each VV on the NP voltage. Therefore, SVV-MPC cannot swiftly restore the NP balance when the NP voltage changes abruptly.

In contrast, TSMPC employs a multilayer structure, where each layer operates independently and corresponds to a specific control objective. This structure ensures that comparisons within each layer are made between variables of similar magnitude. Therefore, regardless of which control objective undergoes a sudden change, the comparison process in the corresponding layer quickly constrains the error to achieve rapid tracking. As a result, the proposed TSMPC exhibits a superior ability to respond quickly to dynamic changes across all control objectives.

In addition, compared to the SMPC in [29] and [30] that limit the number of candidate VVs, the variable number of candidates in the proposed TSMPC ensures that the solution found is optimal. In inverters, especially three-level ones, there may be multiple VVs available for the same voltage. Therefore, if the selection process is based solely on the number of candidates rather than the value of the cost function, there may be instances where two candidate VVs yield the same cost function value, which can be considered an overly strict constraint. This could result in a suboptimal final solution.

For instance, suppose the reference for output voltage is as shown in Fig. 8 and the NP voltage deviation is 0. When the number of candidate VVs is fixed to 2, V_1 and V_8, which have the same cost function of the load voltage, might be selected as the candidates. However, according to the previous analysis, either one will have a significant impact on the NP voltage. Notably, while the cost function of V_{15} is the second smallest, this VVs has no impact on the NP voltage. Therefore, V_{15} is the relatively optimal solution when considering all factors. The proposed TSMPC limits the value of the cost function through the tolerance value rather than restricting the number of candidates, thereby avoiding similar issues of inappropriate constraint relaxation.

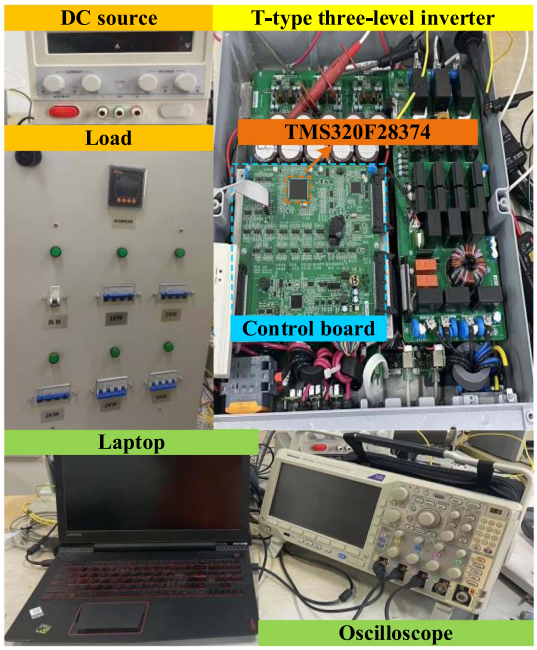

Fig. 9. Experimental platform.

TABLE II
EXPERIMENT PARAMETERS

Symbol	Description	Value
V_{dc}	Dc supply voltage	200 V
C_p, C_n	Dc-link capacitors	100 μF
R	Loads	50 Ω
C	Filter capacitor	40 μF
L	Filter inductance	3.8 mH
f_s	Sampling frequency	16 kHz

V. EXPERIMENTAL RESULTS

To verify the effectiveness of the proposed TSMPC, an experimental platform of a T-type 3P-3L inverter has been established, as shown in Fig. 9, and its parameters are listed in Table II. A 32-bit digital signal processor (DSP) TMS320F28374 is used as the controller, VAC current sensors are used to sample the inverter output current $i_{x(x\ =\ a,b,c)}$ and the load current

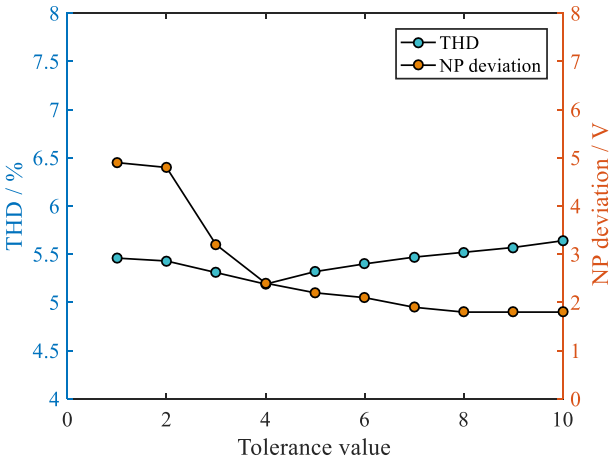

Fig. 10. Specific experimental results of different tolerance values.

$i_{ox(x\,=\,a,b,c)}$, and LEM voltage sensors are used to sample the load voltage $V_{ox(x\,=\,a,b,c)}$ and dc-link capacitor voltages V_p and V_n.

To make the comparison experiments more credible, this article compares C-MPC with weighting factors [19], SVV-MPC [26], [27], and the proposed TSMPC. To ensure fair comparisons of the experiments, numerous a priori experiments have been conducted to compare the THD of the output voltage and NP voltage deviation of C-MPC with different weighting factors. Ultimately, the weighting factor was determined to be 4 to balance the performance of both.

A. Comparison of Tolerance Values

To analyze the impact of tolerance values ε on THD and NP deviation, comparative experiments with different tolerance values have been conducted. The specific experimental results are shown in Fig. 10. When $\varepsilon \leq 2$, the THD and NP deviation are both relatively high. This is because only one VV will fulfill the constraint of the first layer when the tolerance value is excessively low, subsequently leading to the failure of the second layer. Furthermore, the fluctuation in output voltage caused by the fluctuation in NP voltage will result in higher THD. This explains why THD is greater when $\varepsilon \leq 2$ than when ε is set to 4. When $\varepsilon > 2$, as the tolerance value ε increases, the NP deviation decreases, while the THD increases slightly. However, the overall growth of THD is still very small. In addition, it is important to note that an excessively high tolerance value does not result in a significant increase in THD, as the proposed TSMPC requires sector determination. In summary, the proposed TSMPC is effective when ε is chosen appropriately. In subsequent comparative experiments, ε is set to 4.

B. Steady-State Experiments

To compare the steady-state performance of the above-mentioned algorithms, comparative experiments on linear load and nonlinear load were conducted. The specific test conditions are shown below.

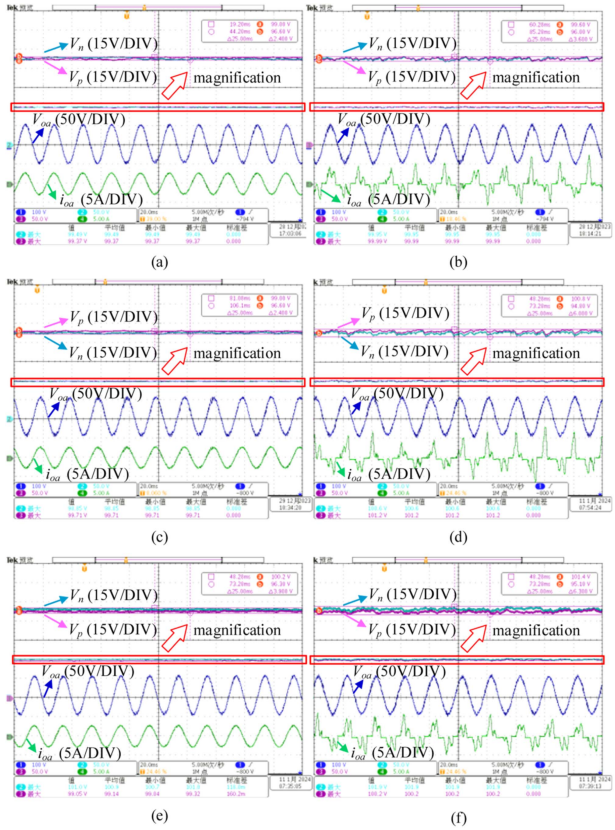

Fig. 11. Steady-state experimental waveforms. (a) TSMPC in Case B1. (b) TSMPC in Case B2. (c) C-MPC in Case B1. (d) C-MPC in Case B2. (e) SVV-MPC in Case B1. (f) SVV-MPC in Case B2.

Case B1: The linear load is 25 Ω resistance.
Case B2: The nonlinear load is an uncontrollable rectifier-type nonlinear load.

The steady-state experimental waveforms of the proposed TSMPC, C-MPC, and SVV-MPC are illustrated in Fig. 11. It contains the load current i_{oa} and voltage V_{oa}, as well as the magnification of dc-link capacitor voltages V_p and V_n. The corresponding harmonic spectrums are illustrated in Fig. 12.

As can be seen in Fig. 11, all three algorithms can accurately track the voltage reference and maintain NP balance. For the proposed TSMPC, C-MPC, and SVV-MPC, the NP deviations are 2.4, 2.4, and 3.9 V under linear load, respectively, compared to 3.6, 6, and 6.3 V under nonlinear load. From Fig. 12, it is found that the corresponding harmonic spectrums are 5.19%, 6.51%, and 5.34% under linear load, respectively, compared to 7.73%, 7.85%, and 7.84% under nonlinear load. It is worth noting that although the THD of the three algorithms is similar, the proposed TSMPC has the smallest NP deviation and the best NP balance effect, while SVV-MPC has the largest NP deviation and the worst NP balance effect. Therefore, the proposed TSMPC has the advantage of excellent NP balance performance.

C. Dynamic Experiments

To compare the dynamic performance of the above three algorithms, comparative experiments of sudden reference voltage

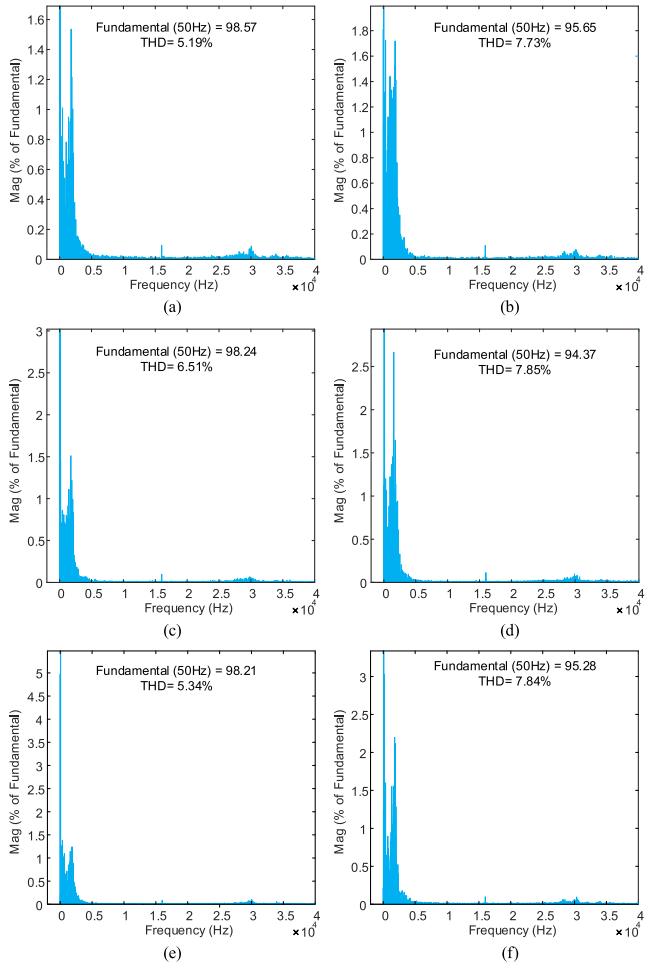

Fig. 12. Steady-state experimental harmonics spectrums. (a) TSMPC in Case B1. (b) TSMPC in Case B2. (c) C-MPC in Case B1. (d) C-MPC in Case B2. (e) SVV-MPC in Case B1. (f) SVV-MPC in Case B2.

change were conducted. The specific test conditions are shown below.

Case C1: The reference voltage increased from 50 to 100 V.
Case C2: The reference voltage decreased from 100 to 50 V.

The dynamic experiment waveforms are illustrated in Fig. 13, with a red circle indicating the position of the sudden increase or decrease in the reference voltage. It can be observed that the proposed TSMPC, C-MPC, and SVV-MPC can accurately track the reference voltage and maintain NP voltage balance, regardless of sudden changes in the reference voltage. For the proposed TSMPC, C-MPC, and SVV-MPC, the time taken to reach a steady state after a reference voltage change is 39.2, 43.5, and 47.2 ms respectively when the reference voltage increased from 50 to 100 V, compared to 43.6, 58.7, and 64.3 ms when the reference voltage decreased from 100 to 50 V. Notably, although all three algorithms can reach the steady state, the proposed TSMPC takes the least time while SVV-MPC takes the most. And the proposed TSMPC has the least NP fluctuation among the three algorithms. Thus, TSMPC exhibits the best dynamic performance.

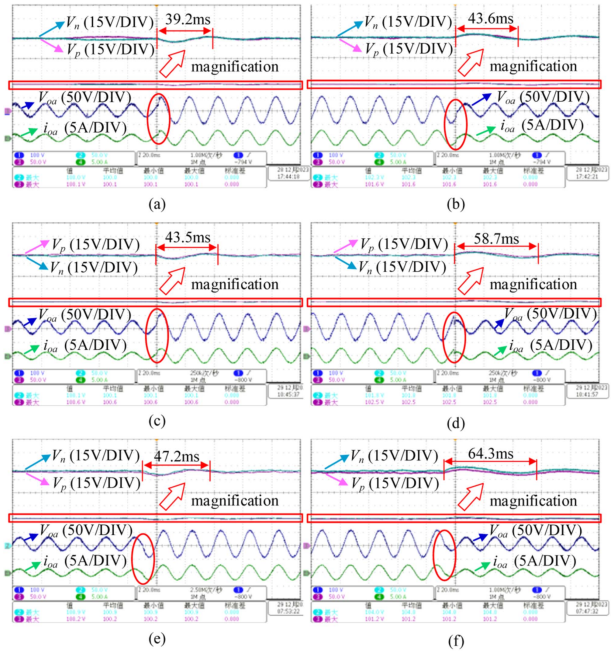

Fig. 13. Dynamic experimental waveforms. (a) TSMPC in Case C1. (b) TSMPC in Case C2. (c) C-MPC in Case C1. (d) C-MPC in Case C2. (e) SVV-MPC in Case C1. (f) SVV-MPC in Case C2.

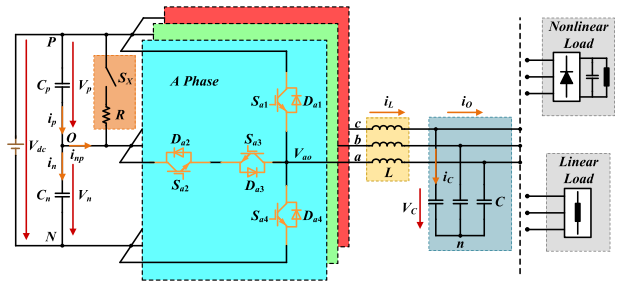

Fig. 14. Schematic diagram simulating NP voltage fluctuation.

D. NP Voltage Balance Experiments

To compare NP voltage balancing performance, a resistor was suddenly paralleled on the upper dc-link capacitor to simulate NP voltage fluctuations, as illustrated in Fig. 14, where the resistor R is 200 Ω, and S_X represents a manual switch. Although this simulation method is relatively extreme, it can better reflect the NP voltage balancing effect of the algorithm. The specific test conditions are as follows.

Case D1: Switch S_X is suddenly closed.
Case D2: Switch S_X is suddenly opened.

The NP voltage balance experimental waveforms are illustrated in Fig. 15, with the positions where switch S_X is closed or opened highlighted by red circles. Observations from Fig. 15 reveal that the proposed TSMPC, C-MPC, and SVV-MPC are effective in managing sudden NP fluctuations and maintaining NP voltage balance. When the switch is suddenly closed, the three algorithms take 13.4, 23.8, and 68.6 ms, respectively, to reach the steady state, with their maximum NP deviations being 3.3, 3.6, and 6.9 V. Conversely, when the switch is suddenly opened,

TABLE III
SPECIFIC PERFORMANCE EVALUATION RESULTS OF THREE ALGORITHMS

	Steady-State performance				Dynamic performance		NP balance performance				Computational burden
Evaluation criteria	THD		Max NP deviation		Time to steady state		Time to steady state		Max NP deviation		Execution time
Working condition	Linear load	Nonlinear load	Linear load	Nonlinear load	Reference increase	Reference decrease	Close switch	Open switch	Close switch	Open switch	
TSMPC	5.19%	7.73%	2.4 V	3.6 V	39.2 ms	43.6 ms	13.4 ms	7.8 ms	3.3 V	2.7 V	53.30 μs
C-MPC	6.51%	7.85%	2.4 V	6 V	43.5 ms	58.7 ms	23.8 ms	8.6 ms	3.6 V	3.6 V	31.55 μs
SVV-MPC	5.34%	7.84%	3.9 V	6.3 V	47.2 ms	64.3 ms	68.8 ms	59.4 ms	6.9 V	4.8 V	20.37 μs

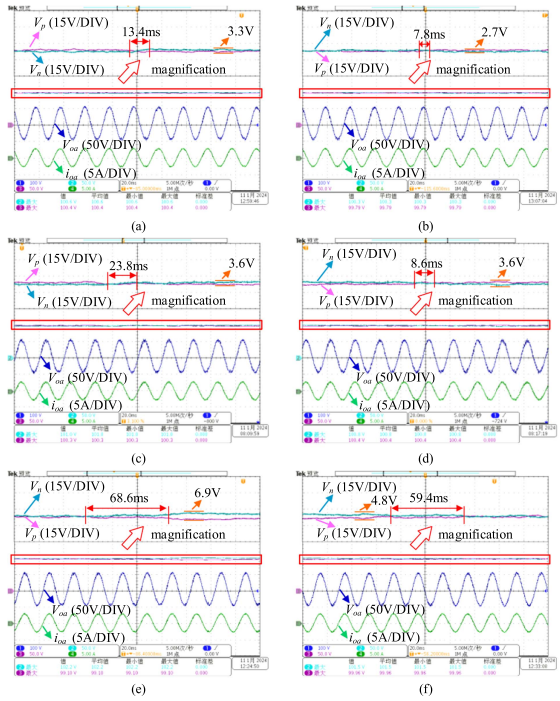

Fig. 15. NP voltage balance experimental waveforms. (a) TSMPC in Case D1. (b) TSMPC in Case D2. (c) C-MPC in Case D1. (d) C-MPC in Case D2. (e) SVV-MPC in Case D1. (f) SVV-MPC in Case D2.

the stabilization times are 7.8, 8.6, and 59.4 ms, with maximum NP deviations of 2.7, 3.6, and 4.8 V, respectively. Notably, the proposed TSMPC reaches a steady state much quicker than the other two algorithms, and it also has the smallest maximum NP deviation. Furthermore, whether the switch S_X is closed or opened, the proposed TSMPC is the only algorithm where NP voltage fluctuations are not significantly visible, demonstrating its superior NP balancing performance.

E. Comparison of Computational Burden

To compare the computational burden of the above algorithms, the execution time of each algorithm was measured using the clock function provided by Code Composer Studio. The specific results are presented in Table III. The execution times of the proposed TSMPC, C-MPC, and SVV-MPC are 53.30, 31.55, and 20.37 μs, respectively.

The proposed TSMPC algorithm employs a multilayer serial screening structure to ensure good dynamic tracking performance for both control objectives. However, compared to the single comparison loop in C-MPC and SVV-MPC, the three comparison loops inherent to this structure significantly increase computational time. Despite this, the proposed TSMPC algorithm mitigates the computational load by reducing the number of candidates in each loop through the sector determination process, thereby keeping the execution time within the DSP's interrupt interval of 62.5 μs (calculated as 62.5 $\mu\text{s} = 1/f_s$, where $f_s = 16$ kHz). This ensures the practical viability of the proposed TSMPC in actual equipment.

F. Overall Comparison of the Experimental Results

To provide a more intuitive comparison of the control performance of the three algorithms, steady-state performance is evaluated using THD and maximum NP deviation under steady-state conditions, dynamic performance is evaluated by the time taken to reach a steady state following a sudden change in reference voltage, NP balance performance is evaluated by the time taken to reach a steady state following a sudden change in NP voltage and the maximum NP deviation, and the computational burden is evaluated by the algorithm's execution time. The specific performance evaluation results of three algorithms are detailed in Table III.

It can be noticed that compared to C-MPC and SVV-MPC, the proposed TSMPC obtains better steady-state performance, superior dynamic performance, and improved NP balance performance, albeit with a slightly higher computational burden. Specifically, in steady-state experiments, the THD and maximum NP deviation of the proposed TSMPC are smaller than those of the other two algorithms. In dynamic experiments, the time taken to reach a steady state is the smallest. In the NP balance experiments, both the time taken to reach a steady state

and maximum NP deviation in the NP balance experiments are the smallest among the three algorithms.

In addition, although the SVV-MPC algorithm has the shortest execution time, its NP balance performance is significantly inferior to that of the other two algorithms. This is particularly evident in the significantly longer time required to reach a steady state following a sudden change in NP voltage. Specifically, when the switch is suddenly closed, SVV-MPC takes approximately 68.8 ms to reach a steady state, which is about 5.13 times longer than the proposed TSMPC and 2.9 times longer than C-MPC. Meanwhile, when the switch is suddenly opened, SVV-MPC takes approximately 59.4 ms to reach a steady state, which is about 7.6 times longer than the proposed TSMPC and 6.9 times longer than C-MPC.

VI. Conclusion

This article proposes a TSMPC based on the lexicographic optimization method for T-type three-phase three-level inverters, aiming to eliminate the weighting factors. The tolerance value in the proposed TSMPC has a more intuitive graphical and textual physical meaning, making the method itself interpretable. Moreover, the use of sector determination not only reduces excessive CPU resource consumption but also prevents anomalies in THD caused by excessively large tolerance values. Finally, comparative experiments with conventional MPC with weighting factors and MPC using redundant small VVs to dynamically maintain NP balance were conducted, demonstrating that the proposed TSMPC not only can accurately track reference voltage but also effectively handle abnormal NP voltage fluctuations, demonstrating its superior control performance in handling dynamic changes across all control objectives.

References

[1] B. Bilgin et al., "Making the case for electrified transportation," *IEEE Trans. Transp. Electrific.*, vol. 1, no. 1, pp. 4–17, Jun. 2015.

[2] S. S. Williamson, A. K. Rathore, and F. Musavi, "Industrial electronics for electric transportation: Current state-of-the-art and future challenges," *IEEE Trans. Ind. Electron.*, vol. 62, no. 5, pp. 3021–3032, May 2015.

[3] S. Vazquez, S. M. Lukic, E. Galvan, L. G. Franquelo, and J. M. Carrasco, "Energy storage systems for transport and grid applications," *IEEE Trans. Ind. Electron.*, vol. 57, no. 12, pp. 3881–3895, Dec. 2010.

[4] B. K. Bose, "Power electronics, smart grid, and renewable energy systems," *Proc. IEEE*, vol. 105, no. 11, pp. 2011–2018, Nov. 2017.

[5] D. Ronanki and S. S. Williamson, "Modular multilevel converters for transportation electrification: Challenges and opportunities," *IEEE Trans. Transp. Electrific.*, vol. 4, no. 2, pp. 399–407, Jun. 2018.

[6] J. Hu, Y. Shan, K. W. Cheng, and S. Islam, "Overview of power converter control in Microgrids—Challenges, advances, and future trends," *IEEE Trans. Power Electron.*, vol. 37, no. 8, pp. 9907–9922, Aug. 2022.

[7] B. Lin, L. Peng, and X. Liu, "Selective pole placement and cancellation for Proportional–Resonant control design used in voltage source inverter," *IEEE Trans. Power Electron.*, vol. 37, no. 8, pp. 8921–8934, Aug. 2022.

[8] M. Parvez, M. F. M. Elias, N. A. Rahim, F. Blaabjerg, D. Abbott, and S. F. Al-Sarawi, "Comparative study of discrete PI and PR controls for single-phase UPS inverter," *IEEE Access*, vol. 8, pp. 45584–45595, 2020.

[9] M. Ö. Efe, "Fractional order systems in industrial automation—A survey," *IEEE Trans. Ind. Inf.*, vol. 7, no. 4, pp. 582–591, Nov. 2011.

[10] J. Han, "From PID to active disturbance rejection control," *IEEE Trans. Ind. Electron.*, vol. 56, no. 3, pp. 900–906, Mar. 2009.

[11] N. Monshizadeh, F. Mancilla-David, R. Ortega, and R. Cisneros, "Nonlinear stability analysis of the classical nested PI control of voltage sourced inverters," *IEEE Control Syst. Lett.*, vol. 6, pp. 1442–1447, 2022.

[12] H.-S. Kim, Y.-C. Kwon, S.-J. Chee, and S.-K. Sul, "Analysis and compensation of inverter nonlinearity for three-level T-type inverters," *IEEE Trans. Power Electron.*, vol. 32, no. 6, pp. 4970–4980, Jun. 2017.

[13] J. Rodriguez et al., "Latest advances of model predictive control in electrical drives—Part II: Applications and benchmarking with classical control methods," *IEEE Trans. Power Electron.*, vol. 37, no. 5, pp. 5047–5061, May 2022.

[14] P. Karamanakos, E. Liegmann, T. Geyer, and R. Kennel, "Model predictive control of power electronic systems: Methods, results, and challenges," *IEEE Open J. Ind. Appl.*, vol. 1, pp. 95–114, 2020.

[15] S. Vazquez, J. Rodriguez, M. Rivera, L. G. Franquelo, and M. Norambuena, "Model predictive control for power converters and drives: Advances and trends," *IEEE Trans. Ind. Electron.*, vol. 64, no. 2, pp. 935–947, Feb. 2017.

[16] J. I. Leon, S. Vazquez, and L. G. Franquelo, "Multilevel converters: Control and modulation techniques for their operation and industrial applications," *Proc. IEEE*, vol. 105, no. 11, pp. 2066–2081, Nov. 2017.

[17] M. Schweizer and J. W. Kolar, "Design and implementation of a highly efficient three-level T-type converter for low-voltage applications," *IEEE Trans. Power Electron.*, vol. 28, no. 2, pp. 899–907, Feb. 2013.

[18] E. C. Kerrigan and J. M. Maciejowski, "Designing model predictive controllers with prioritised constraints and objectives," in *Proc. IEEE Int. Symp. Comput. Aided Control System Des.*, 2002, pp. 33–38.

[19] J. Rodriguez et al., "Latest advances of model predictive control in electrical drives—Part I: Basic concepts and advanced strategies," *IEEE Trans. Power Electron.*, vol. 37, no. 4, pp. 3927–3942, Apr. 2022.

[20] P. Cortes et al., "Guidelines for weighting factors design in model predictive control of power converters and drives," in *Proc. IEEE Int. Conf. Ind. Technol.*, 2009, pp. 1–7.

[21] L. Tang et al., "Model predictive thrust control for linear induction machine: A fuzzy optimization approach," *IEEE Trans. Ind. Appl.*, vol. 59, no. 2, pp. 2532–2545, Mar./Apr. 2023.

[22] A. Oshnoei and F. Blaabjerg, "Sliding mode-based model predictive control of grid-forming power converters," in *Proc. Eur. Control Conf.*, 2023, pp. 1–6.

[23] F. Wang et al., "Design of model predictive control weighting factors for PMSM using Gaussian distribution-based particle swarm optimization," *IEEE Trans. Ind. Electron.*, vol. 69, no. 11, pp. 10935–10946, Nov. 2022.

[24] P. R. U. Guazzelli, W. C. de Andrade Pereira, C. M. R. de Oliveira, A. G. de Castro, and M. L. de Aguiar, "Weighting factors optimization of predictive torque control of induction motor by multiobjective genetic algorithm," *IEEE Trans. Power Electron.*, vol. 34, no. 7, pp. 6628–6638, Jul. 2019.

[25] T. Dragičević and M. Novak, "Weighting factor design in model predictive control of power electronic converters: An artificial neural network approach," *IEEE Trans. Ind. Electron.*, vol. 66, no. 11, pp. 8870–8880, Nov. 2019.

[26] Y. Yang, H. Wen, M. Fan, M. Xie, and R. Chen, "Fast finite-switching-state model predictive control method without weighting factors for T-type three-level three-phase inverters," *IEEE Trans. Ind. Inf.*, vol. 15, no. 3, pp. 1298–1310, Mar. 2019.

[27] Y. Yang, H. Wen, M. Fan, M. Xie, R. Chen, and Y. Wang, "A constant switching frequency model predictive control without weighting factors for T-type single-phase three-level inverters," *IEEE Trans. Ind. Electron.*, vol. 66, no. 7, pp. 5153–5164, Jul. 2019.

[28] C. A. Rojas, J. Rodriguez, F. Villarroel, J. R. Espinoza, C. A. Silva, and M. Trincado, "Predictive torque and flux control without weighting factors," *IEEE Trans. Ind. Electron.*, vol. 60, no. 2, pp. 681–690, Feb. 2013.

[29] M. Norambuena, J. Rodriguez, Z. Zhang, F. Wang, C. Garcia, and R. Kennel, "A very simple strategy for high-quality performance of AC machines using model predictive control," *IEEE Trans. Power Electron.*, vol. 34, no. 1, pp. 794–800, Jan. 2019.

[30] Y. Zhang, B. Zhang, H. Yang, M. Norambuena, and J. Rodriguez, "Generalized sequential model predictive control of IM drives with field-weakening ability," *IEEE Trans. Power Electron.*, vol. 34, no. 9, pp. 8944–8955, Sep. 2019.

[31] M. Anilkumar, N. Padhiyar, and K. Moudgalya, "Lexicographic optimization based MPC: Simulation and experimental study," *Comput. Chem. Eng.*, vol. 88, pp. 135–144, May 2016.

[32] C. Ocampo-Martinez, A. Ingimundarson, V. Puig, and J. Quevedo, "Objective prioritization using lexicographic minimizers for MPC of sewer networks," *IEEE Trans. Control Syst. Technol.*, vol. 16, no. 1, pp. 113–121, Jan. 2008.

[33] K. Zhang et al., "Tolerant sequential model predictive direct torque control of permanent magnet synchronous machine drives," *IEEE Trans. Transp. Electrific.*, vol. 6, no. 3, pp. 1167–1176, Sep. 2020.

Shengwei Chen received the B.S. degree in electrical engineering from Soochow University, Suzhou, China, in 2021, and the M.S. degree in transportation engineering from Soochow University, Suzhou, China, in 2024. He is currently working toward the Ph.D. degree in electrical engineering from the College of Electrical Engineering, Zhejiang University, Hangzhou, China.

His research interest includes power electronic technology and model predictive control.

Yong Yang (Senior Member, IEEE) received the B.S. degree in automation from Xiangtan University, Xiangtan, China, in 2003, the M.S. degree in electrical engineering from Guizhou University, Guiyang, China, in 2006, and the Ph.D. degree in electrical engineering from Shanghai University, Shanghai, China, in 2010.

He is currently a full Professor with the School of Rail Transportation, Soochow University. From December 2017 to December 2018, he was a Visiting Scholar with the Center for High Performance Power Electronics (CHPPE) of The Ohio State University, Columbus, USA. He has coauthored more than 100 journal and conference papers. His current research interests include model predictive control in power electronic converters, distributed energy resource interfacing, and high-performance motor drive control.

Rong Chen was born in Jiangsu, China, in 1983. She received the B.S. degree in communication engineering, the M.S. degree in communication and information system, and the Ph.D. degree in signal and information processing from Soochow University, Suzhou, China, in 2006, 2009, and 2013, respectively.

She is currently an Associate Professor with the School of Rail Transportation, Soochow University. Her research interests include signal processing and synchronous phasor measuring.

Jiefeng Hu (Senior Member, IEEE) received the Ph.D. degree in electrical engineering from University of Technology Sydney (UTS), Ultimo, Australia, in 2013.

He participated in the research of minigrids in Commonwealth Scientific and Industrial Research Organization, Newcastle, Australia. He was an Assistant Professor with The Hong Kong Polytechnic University, Kowloon, Hong Kong. He is currently an Associate Professor and a Program Coordinator of Electrical Engineering with Federation University Australia, Ballarat, VIC, Australia, where he is also the Stream Leader of Centre for New Energy Transition Research. His research interests include power electronics, renewable energy, and smart microgrids.

Dr. Hu is an Associate Editor for IET Renewable Power Generation, an Editor for IEEE TRANSACTIONS ON ENERGY CONVERSION, an Associate Editor for IEEE ACCESS, and was a Guest Editor for IEEE TRANSACTIONS ON INDUSTRIAL ELECTRONICS for a Special Issue "Applications of Predictive Control in Microgrids."

Huiqing Wen (Senior Member, IEEE) received the B.S. and M.S. degrees in electrical engineering from Zhejiang University, Hangzhou, China, in 2002 and 2006, respectively, and the Ph.D. degree in electrical engineering from the Chinese Academy of Sciences, Beijing, China, in 2009.

From 2009 to 2010, he was an Electrical Engineer with the Research and Development Center, GE (China) Co., Ltd., Shanghai, China. From 2010 to 2011, he was an Engineer with the China Coal Research Institute, Beijing, China. From 2011 to 2012, he was a Postdoctoral Fellow with the Masdar Institute of Science and Technology, Abu Dhabi, United Arab Emirates. He is presently working as a Professor with the Xi'an Jiaotong-Liverpool University, Suzhou, China. His current research interests include bidirectional dc–dc converters, power electronics in flexible ac transmission applications, electrical vehicles, and high-power, three-level electrical driving systems.

Yiwang Wang (Member, IEEE) received the B.S. degree in electrical engineering and automation from the Kunming University of Science and Technology, Kunming, China, in 2005, the M.S. degree in power electronics from Jiangnan University, Wuxi, China, in 2008, and the Ph.D. degree in electrical engineering from Shanghai Jiao Tong University, Shanghai, China, in 2020.

He is currently a Professor with the Collaborative Innovation Center of Smart Energy Equipment and Power Conversion, Suzhou Vocational University, Suzhou, China. He is also a Director of Suzhou Key Laboratory of Smart Energy Technology. His research interests include power electronics intelligence control, and the applications of power electronics and renewable energy.

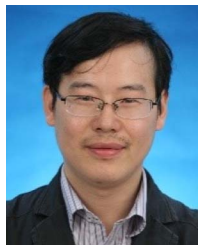

Weimin Wu (Member, IEEE) received Ph.D. degree in electrical engineering from the College of Electrical Engineering, Zhejiang University, Hangzhou, China, in 2005.

He worked as a Research Engineer with the Delta Power Electronic Center (DPEC), Shanghai, from July, 2005 to June, 2006. Since July, 2006, he has been a Faculty Member with Shanghai Maritime University, where he is currently a Full Professor with the Department of Electrical Engineering. He was a Visiting Professor with the Center for Power Electronics Systems (CPES), Virginia Polytechnic Institute and State University, Blacksburg, USA, from September 2008 to March 2009. From November 2011 to January 2014, he was also a visiting Professor with the Department of Energy Technology, Aalborg University, Aalborg, Demark, working with the Center of Reliable Power Electronics (CORPE). He has coauthored more than 180 papers and holds eighteen patents. His research interests include power converters for renewable energy systems, power quality, smart grid, and energy storage technology.

Dr. Wu serves as an Associate Editor for IEEE TRANSACTIONS ON INDUSTRY ELECTRONICS.

Gang Fang (Member, IEEE) received the B.S. degree in electrical engineering from the Beijing Jiaotong University, Beijing, China, in 2006.

He has been working as a Deputy General Manager with the GOODWE Technology Company, Ltd., since 2010. His research interests include the design and control of power converters and solar power systems.

Jose Rodriguez (Life Fellow, IEEE) received the Engineer degree in electrical engineering from the Universidad Tecnica Federico Santa Maria, in Valparaiso, Chile, in 1977, and the Dr.-Ing. degree in electrical engineering from the University of Erlangen, Erlangen, Germany, in 1985.

He has been with the Department of Electronics Engineering, Universidad Tecnica Federico Santa Maria, since 1977, where he was full Professor and President. From 2015 to 2019, he was the President of Universidad Andres Bello in Santiago, Chile. Since 2022, he has been the President of Universidad San Sebastian in Santiago, Chile. He has coauthored two books, several book chapters, and more than 700 journal and conference papers. His main research interests include multilevel inverters, new converter topologies, control of power converters, and adjustable-speed drives.

Dr. Rodriguez was the recipient of a number of best paper awards from journals of the IEEE. He was also the recipient of the National Award of Applied Sciences and Technology from the government of Chile, in 2014 and the Eugene Mittelmann Award from the Industrial Electronics Society of the IEEE, in 2015. In years 2014 to 2021, he has been included in the list of Highly Cited Researchers published by Web of Science. He is a member of the Chilean Academy of Engineering.